J Eng Math (2008) 61:285–300
DOI 10.1007/s10665-007-9184-0

Thermo-Elastic Dynamic Instability (TEDI)—a review of recent results

Luciano Afferrante · Michele Ciavarella

Received: 9 November 2006 / Accepted: 6 August 2007 / Published online: 12 September 2007

Abstract Frictional instabilities arise in a number of engineering and scientific contexts, when the presence of friction renders unstable the uniform motion between parts under nominally uniform conditions. Various classes of friction instabilities exist, those involving friction weakening with speed, and those at constant coefficient of friction. In the latter class, in turn, there are Dynamic Instabilities (DI) and Thermo-Elastic Instabilities (TEI). Recently, by including inertia terms in the formulations of the simple models already studied, the merging of TEI and DI has shown that, although the coupling of dynamic and thermal terms is generally weak (given the significant difference in the typical time scales of the two processes), thermal effects are capable of making otherwise neutrally stable dynamic modes unstable, rendering the new form of instability TEDI (ThermoElastoDynamic Instability) potentially interesting in a number of applications. Some results involving 1D and 2D models of TEDI are reviewed.

Keywords Dynamic instability · Frictional vibrations · Squeal · Thermo-elastic contact · Thermo-elastic instability

1 Introduction

Frictional instabilities in the sliding of elastic bodies are complex phenomena resulting from the interaction between relatively simple physical processes, notably the elastic deformation of contacting bodies, the development of frictional forces at the interface opposing the motion and the consequent generation of frictional heat. These instabilities are of interest in a wide range of scientific and industrial applications. In the sliding of tectonic plates during earthquakes [1,2], Dynamic Instabilities (DI) are believed to have a crucial role in the sliding events. Dynamic Instabilities are also at play in the sliding of rubber-like materials [3], or in *squeal*, a typical problem of brake systems. Such brake noise is a vehicle system problem and the severity, regularity and tone is generally unacceptable for road use. The contact between the pad and disk during braking creates the raw energy to produce the noise, but the actual squeal can be primarily a combination of the disk, caliper and pad? A number of methods are available to reduce the noise factor of a brake system, but the reduction or elimination of noise is usually achieved by a process of trial and error. Friction instabilities are generally held responsible for squeal. However, there is a large body of literature

L. Afferrante (✉) · M. Ciavarella
CEMEC-PoliBA—Centre of Excellence in Computational Mechanics, V.le Japigia 182, Politecnico di Bari, 70125 Bari Italy
e-mail: luciano@poliba.it

devoted to developing models that explain brake squeal and determine its dependence on the parameters of the brake system [4,5].

Hoffmann and Gaul [6] recently showed that instability occurs for cases when the system has no static steady sliding-state solution, which is closely related to a phenomenon first discovered by Painlevé when considering sliding rigid bodies. This is called the "Painlevé paradox" [7,8]. Instability is related to loss of existence, but this is not always the case. The key factor in friction-excited vibrations has been often considered to be the "rate weakening", i.e., the negative slope of the friction–velocity curve [9,10]. This negative friction-curve slope manifests itself in dynamic systems as a negative viscous-damping term, which has a destabilizing effect. Rabinowicz [10] first put forward the idea of memory-dependent friction, in which a time lag of friction response is observed. He proposed that only after sliding a critical distance would friction evolve to its steady-state value at that particular system's sliding speed. As a result, the instantaneous slope of the friction curve is actually a multi-valued function which depends upon the previous sliding history [9,11,12]. Hunt et al. [13] performed experiments on steady sliding of machine tools and concluded that velocity dependence of friction alone could not account for all observed effects. Popp [14] reviews some model problems for stick–slip oscillations and chaotic response in dry sliding. He uses four different friction laws with four different system-dynamic models and reports on the nonlinear response and bifurcation behavior under various operating conditions. He concluded that even (structurally) linear systems can demonstrate a nonlinear response due to the nonlinear friction force.

In addition to velocity-dependent friction, the role of normal-tangential coupling in system dynamics has been examined as a contributor to steady-sliding instability or stick–slip oscillations. The first work in this area was done by Tolstoi [15], who completed delicate experiments which measured both the in-plane (tangential) motion, as well as the out-of-plane (normal) motion of a slider against a counter-surface. He noticed tangential slip events were invariably accompanied by simultaneous upward normal motion; a normal-contact resonance condition could be observed under which apparent friction was reduced. The argument here is that, in order for friction to change, the real area of contact must change, and therefore the mean normal separation of the surfaces must also change. A similar idea to Tolstoi's was that of Godfrey [16]. He demonstrates an apparent friction reduction due to normal vibrations: normal vibrations influence the mean surface separation, and therefore the real area of contact. With the measured frictional shear being a function of real contact area, there is an apparent reduction in friction force with normal vibration. Also, Sakamoto [17] used a pin-on-disk configuration to examine normal separation effects in sliding contacts. Friction–velocity loops are observed, and the variation in friction is interpreted as a change in the real area of contact during sliding (as inferred from contact-resistance measurements).

Another class of instabilities is due to frictional heating. In such cases, thermo-elastic deformation of the contacting bodies modifies the contact pressure distribution and can lead to a rich variety of phenomena including localization and DI. These effects are of considerable technological importance, including, for example, brakes and clutches in automotive applications. Such a phenomenon is known as Frictionally excited Thermo-elastic Instability (TEI) [18–22]. The most important consequence of TEI is the formation of hot spots at the sliding interface - hot spots can cause in turn material damage and wear and are also a source of undesirable frictional vibrations, known in the automotive disk-brake community as "hot roughness" or "hot judder" [23–27]. In this process, any perturbation in contact pressure causes a corresponding perturbation in heating and hence thermal distortion, which exaggerates the initial perturbation. It has received more attention in technological applications for which it is of critical importance, like in the design of brakes and clutches [19,26]. This is due to a coupling between thermal and mechanical contact boundary conditions, for which the product of friction coefficient and speed (and not just friction, as in the DI) acts as a gain in the feedback process. Thus, we anticipate that, for a given friction coefficient, there will be some sliding speed, V_{cr}, above which the system will be unstable.

Burton et al. [28] used a perturbation method to investigate the stability of contact between two sliding half-planes. The system is linearized about the uniform pressure state and perturbations are sought that can grow exponentially in time. Their results provided useful insight into the nature of the phenomenon, but there is no inherent length scale in the problem as defined and it was found that sufficiently long wavelengths are always unstable. A length scale can be artificially introduced into the analysis by restricting attention to perturbations below a certain wavelength, estimated as being comparable with the linear dimensions of the practical system; however, the resulting

predictions for critical speed do not generally show good agreement with those observed experimentally [29,30]. The first solution of a TEI problem involving a geometric length scale was given by Lee and Barber [31], who used Burton's method to analyze the stability of a layer sliding between two half-planes. This geometry provided a first step towards that of the typical disk-brake assembly, where a disk slides between two pads of a frictional material. Using typical material properties from automotive applications, it was found that stability is governed by a deformation mode that is antisymmetric with respect to the mid-plane of the layer and has a wavelength proportional to the layer thickness. Despite the considerable idealizations involved in Lee's theory, it provides plausible predictions for the critical speed and the mode shape in typical brake assemblies and is therefore quite widely used in the brake and clutch industry for TEI analysis. However, this method does not account for other features of the system geometry, such as the finite width of the sliding surface, the axisymmetric geometry of the disk and the 'hat' section used to attach the disk to its support. One approach is to use the finite-element method to solve the coupled transient thermo-elastic contact problem in time [25,32,33]. This method is extremely flexible, in that it can accommodate nonlinear or temperature-dependent constitutive behavior, more realistic friction laws and practical loading cycles. However, it is also extremely computer-intensive and appears unlikely to be a practical design tool for three-dimensional problems in the foreseeable future.

Recently, Yi et al. [34] developed a strategy to solve thermo-elastic instability problems using Fourier reduction. This method was implemented in a finite-element software package (`HotSpotter`) for evaluating the susceptibility of axisymmetric multidisk brakes and clutches toTEI by Yi and Barber [35].

So far, TEI and DI were considered separately (TEI is quasi-static and DI includes no thermal effects). In recent papers, we tried to propose a coupled theory, which we call TEDI (Thermo-Elastic Dynamic Instability).

2 Governing equations

According to the theory of Biot [36] (see also e.g. [37,38]) the governing equations for linear isotropic coupled thermoelastodynamic problems are:

$$K\nabla^2\theta - \rho c_E \frac{\partial\theta}{\partial t} - \alpha\,(3\lambda + 2\mu)\,T_0 \frac{\partial\,(\nabla\cdot\mathbf{u})}{\partial t} = 0, \tag{1}$$

$$\mu\nabla^2\mathbf{u} + (\lambda+\mu)\,\nabla\,(\nabla\cdot\mathbf{u}) - \alpha\,(3\lambda+2\mu)\,\nabla\theta - \rho\frac{\partial^2\mathbf{u}}{\partial t^2} = 0, \tag{2}$$

$$\sigma - \mu\,(\nabla\mathbf{u} + \mathbf{u}\nabla) - \lambda\,(\nabla\cdot\mathbf{u})\,\mathbf{I} + \alpha\,(3\lambda+2\mu)\,\theta\mathbf{I} = 0, \tag{3}$$

$$\mathbf{q} + K\nabla\theta = 0, \tag{4}$$

where (1) is the couple heat equation, (2) is the equation of motion, (3) is the constitutive law and (4) is the heat-conduction equation. Also, in the above equations, σ is the stress tensor, $\mathbf{u}$ is the displacement vector, $\theta = T - T_0$ is the change in temperature, T is the current temperature, T_0 is the initial temperature, $\mathbf{q}$ is the heat-flux vector, λ and μ are the Lamè constants, α is the coefficient of linear thermal expansion, ρ is the mass density, c_E is the specific heat at constant deformation, K is the thermal conductivity, $\mathbf{I}$ is the identity tensor, ∇ is the gradient operator and ∇^2 is the Laplace operator.

We shall review some relevant results of simple (1D and 2D) models for which the above equations can be simplified.

3 "Frictional" and "frictionless" TEDI in a 1D elastic layer

Afferrante et al. [39] and Afferrante and Ciavarella [40,41] found, for a one-dimensional elastic layer sliding against a rigid half-space, that the extremely weak coupling between the elastodynamic and thermo-elastic effects destabilizes the elastodynamic natural vibration modes, causing the system to be unstable at arbitrarily low speeds.

In particular, the model introduced in [39] and [40] was called "frictionless TEDI", since frictional traction was neglected in the analysis for their elastic effects. Also, the elastic layer was considered bonded to the rigid half-space A in [39], and constrained in [40], respectively.

In [41] it was shown that shear tractions at the interface produce deformations in the form of stick–slip waves which interact with the jumping mode of the "frictionless TEDI" , reducing it or completely suppressing it and, for this reason, the authors referred to this as "frictional TEDI".

Here, we shall report only the main results; for a more complete discussion of the formulation we refer to the above-cited papers.

Figure 1 shows an elastic layer $0 < x < h$ which is constrained to a stationary rigid plane A at $x = 0$. A second rigid body B moves to the right at velocity V_0 and its plane surface makes sliding contact with the layer at $x = h$. We also assume that body A is maintained at a temperature $\theta = 0$ and that the sliding body B is a non-conductor, so that all the heat generated by friction flows through the layer.

For plane strain, the governing equations of the problem sketched in Fig. 1 (neglecting the coupled term in the heat-conduction equation, because for typical values the effect is negligible as shown in [42]) write (see also [40,41]):

- heat-conduction equation

$$\frac{\partial^2\theta}{\partial x^2} - \frac{1}{k}\frac{\partial\theta}{\partial t} = 0; \tag{5}$$

- equations of motion

$$\frac{\partial\sigma_{xx}}{\partial x} - \rho\frac{\partial^2 u_x}{\partial t^2} = 0, \tag{6}$$

$$\frac{\partial\sigma_{xy}}{\partial x} - \rho\frac{\partial^2 u_y}{\partial t^2} = 0; \tag{7}$$

- constitutive law of the material

$$\sigma_{xx} = \frac{2\mu(1-\nu)}{1-2\nu}\frac{\partial u_x}{\partial x} - \frac{2\mu(1+\nu)\alpha\theta}{1-2\nu}, \tag{8}$$

$$\sigma_{xy} = \mu\frac{\partial u_y}{\partial x}, \tag{9}$$

where u_x and u_y are the longitudinal and shear displacement; σ_{xx} and σ_{xy} are the normal and shear stress, ν is the Poisson ratio and k is the thermal diffusivity of the material.

Further, the instantaneous sliding speed V is defined as

$$V = V_0 - \frac{\partial u_y}{\partial t}(h, t), \tag{10}$$

where V_0 is the speed of the rigid body B.

To solve the heat-conduction equation (5) we can consider that the end $x = 0$ of the layer is maintained at a temperature $\theta = 0$ and at the other end ($x = h$) the heat generated by friction flows through the layer ($K\partial\theta/\partial x = V\sigma_{xy}$).

To solve the equations of motion (6, 7) four cases of boundary conditions can be considered, as summarized in Table 1:

The stability of the system can be studied by considering the possibility that a small perturbation in the temperature, stress and displacement fields can grow exponentially in time [28,43]. A complete picture of the characteristic

Table 1 Possible cases of constraint

	Normal force	Normal displacement
Tangential force	NF–TF	ND–TF
Tangential displacement	NF–TD	ND–TD

equations is given in [44]. Here we turn our attention to the cases with tangential-displacement constraint because similar conclusions can be drawn for the other ones.

When the normal force and the tangential displacement are constrained (NF–TD), the characteristic equation takes the form

$$f\frac{H}{2\beta^{3/2}}\left\{\sqrt{\beta}\hat{V}_0\cosh\left(\tilde{b}/\sqrt{\beta}\right)-f\hat{p}_0\sinh\left(\tilde{b}/\sqrt{\beta}\right)\right\}\frac{\sinh\left(\tilde{b}\right)-\sqrt{\gamma\tilde{b}}\cosh\left(\tilde{b}\right)\tanh\left(\sqrt{\frac{\tilde{b}}{\gamma}}\right)}{1-\gamma\tilde{b}}$$
$$=\cosh\left(\tilde{b}\right)\cosh\left(\tilde{b}/\sqrt{\beta}\right) \tag{11}$$

where f is the friction coefficient, $\beta=\frac{1-2\nu}{2(1-\nu)}$, $H=\frac{2\mu\alpha(1+\nu)k}{K(1-\nu)}$, $\gamma=k/ch$ is an thermoelastodynamic parameter, c is the dilatational wave speed, $\hat{V}_0=V_0/c$ is the dimensionless sliding speed, $\hat{p}_0=\beta p_0/\mu$ is the dimensionless contact pressure and $\tilde{b}=\gamma b=bh/c$ is the dimensionless growth rate.

If we neglect the effect of frictional tractions on normal displacements (i.e., we use 'Goodman's approximation'), we recover the characteristic equation for the limiting "frictionless" TEDI case

$$f\frac{H}{2\gamma\beta}\hat{V}_0=f\hat{V}=\frac{1}{\gamma}\frac{\left(1-\gamma^2b\right)\cosh\left(\sqrt{b}\right)\cosh\left(\gamma b\right)}{\cosh\left(\sqrt{b}\right)\sinh\left(\gamma b\right)-\gamma\sqrt{b}\sinh\left(\sqrt{b}\right)\cosh\left(\gamma b\right)}. \tag{12}$$

This coincides with the characteristic equation found in [40]. In this case, the pure dynamic roots (which represent the natural frequencies of undamped vibration of the system in the absence of thermal expansion) are pushed into the positive half-plane (i.e., acquire positive real part), as a result of the thermal effect.

When the normal and tangential displacements are constrained (NT–TD), the characteristic equation is

$$f\frac{H}{2\beta^{3/2}}\left\{\sqrt{\beta}\hat{V}_0\cosh\left(\tilde{b}/\sqrt{\beta}\right)-f\frac{2H\gamma\hat{\Delta}}{4\gamma\beta-fH\hat{V}_0}\sinh\left(\tilde{b}/\sqrt{\beta}\right)\right\}\frac{\cosh\left(\tilde{b}\right)-1-\sqrt{\gamma\tilde{b}}\sinh\left(\tilde{b}\right)\tanh\left(\sqrt{\frac{\tilde{b}}{\gamma}}\right)}{1-\gamma\tilde{b}}$$
$$=\sinh\left(\tilde{b}\right)\cosh\left(\tilde{b}/\sqrt{\beta}\right) \tag{13}$$

where $\hat{\Delta}=\Delta/h$ is the dimensionless displacement at the end $x=h$ of the layer. In particular, Δ is a small amount with the undeformed thickness of the layer at temperature $T(x)=0$ exceeding h so as to ensure an initial contact pressure at the interface. The limiting "frictionless" TEDI case can be obtained by neglecting the friction:

$$f\frac{H}{2\gamma\beta}\hat{V}_0=f\hat{V}=\frac{1}{\gamma}\frac{\left(1-\gamma^2b\right)\cosh\left(\sqrt{b}\right)\sinh\left(\gamma b\right)}{\cosh\left(\sqrt{b}\right)\cosh\left(\gamma b\right)-1-\gamma\sqrt{b}\sinh\left(\sqrt{b}\right)\sinh\left(\gamma b\right)} \tag{14}$$

coinciding with (2.28) by [39].

3.1 Results

3.1.1 "Frictionless" TEDI

Originally, in [39] we neglected shear waves (i.e., the shear tractions produced at the interface) and, by considering the coupled problem of thermo-elastic deformation in the dynamic formulation, we discovered a new form of instability. In particular, when considering displacement control in the normal direction, we have a TEI critical speed, and the results show a new instability (giving rise in the long run to jumps and impacts at the interface), that is, predicted by an exponential growth rate in Fig. 2, which is plotted against the sliding speed for the first mode ($n=1$), this being the dominant one. The instability originates at any speed and surprisingly is also present for

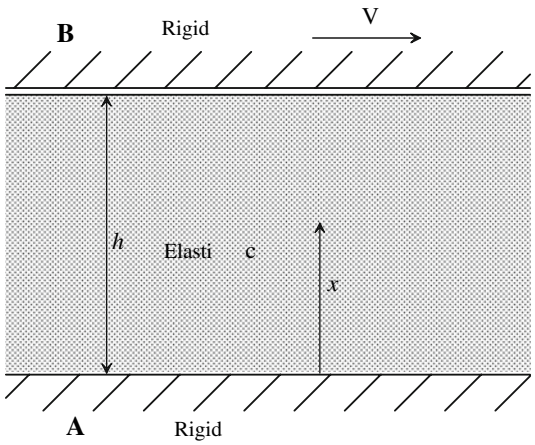

Fig. 1 An elastic layer bounded to a rigid body at $x = 0$ and sliding against a rigid plane surface at $x = h$

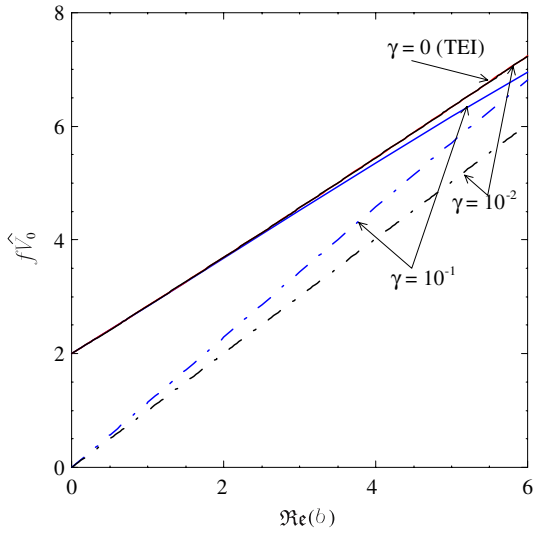

Fig. 2 Frictionless TEDI growth factors for displacement control (from [39])

systems having very different characteristic times of the thermal and dynamic phenomena. In Fig. 2, we plot with a dashed–dot line the real part $\Re\mathfrak{e}\,(b)$ of the complex growth rates, i.e., growth rates with non-zero imaginary part ($b = \Re\mathfrak{e}\,(b) + \mathrm{i}\Im\mathfrak{m}\,(b)$), whereas with a solid line the growth rates with $\Im\mathfrak{m}\,(b) = 0$ ($b = \Re\mathfrak{e}\,(b)$) are denoted. Notice that the real zero passes into the complex plane at the value $\hat{V} = 2$, exactly as in the limiting case $\gamma = 0$. This is to be expected, since a real zero with $\Re\mathfrak{e}(b) = 0$ involves no variation of the stress or temperature perturbations in time and hence the acceleration terms in the governing equations make no contribution. Thus, the elastodynamic properties of the system have no effect on the stability boundary, if this is determined by a real zero.

If we control the normal force, we find similar instabilities, but the pure TEI modes disappear (in Fig. 3 we have only complex growth factors), since in the normal direction, a quasi-static solution (like done in TEI) predicts a trivial solution which we cannot perturb in terms of pressure by definition.

Hence, arbitrarily small amounts of thermoelastodynamic coupling are sufficient to cause undamped oscillatory states to grow in time. The problem remains linear as long as contact is maintained at the sliding end of the rod, so we must conclude that these perturbations will continue to grow exponentially until they are of sufficient amplitude to cause periods of separation.

When the layer is bonded to the half-space $A(u\,(h,t) = -\Delta)$, the results are qualitatively different depending on whether $\hat{V}$ is greater or less than the TEI critical speed $\hat{V}_{\mathrm{cr}} = 2$. In fact, for $\hat{V} > \hat{V}_{\mathrm{cr}}$ we expect that the system tends to a state of thermo-elastic seizure. However, more interesting from an engineering perspective is the range $0 < \hat{V} < 2$ in which the quasi-static solution predicts a monotonic transition to the steady state, but the elastodynamic solution predicts unstable growing oscillations. The transient results show an initial trend similar to the quasi-static prediction with a superposed oscillation whose amplitude grows in time. Eventually, the contact pressure falls to zero and the system undergoes alternating periods of contact and separation tending asymptotically to a limit cycle as shown in Fig. 4.

Notice the period between successive impacts ($\hat{t}_0 = 2\gamma$) is independent of $\hat{V}$ because it represents the time taken for a pressure wave to propagate across the layer and be reflected back to the interface. Similar results can be obtained for other speeds in the range $\hat{V} < 2$, where the quasi-static solution is stable.

By increasing the sliding speed, the maximum contact pressure $p_{\max}$ during the contact phase increases, but the contact period t_c decreases, so the average contact pressure will increase more slowly than the maximum one. Figure 5 shows the variation of the average contact pressure with the sliding speed (the steady-state contact pressure

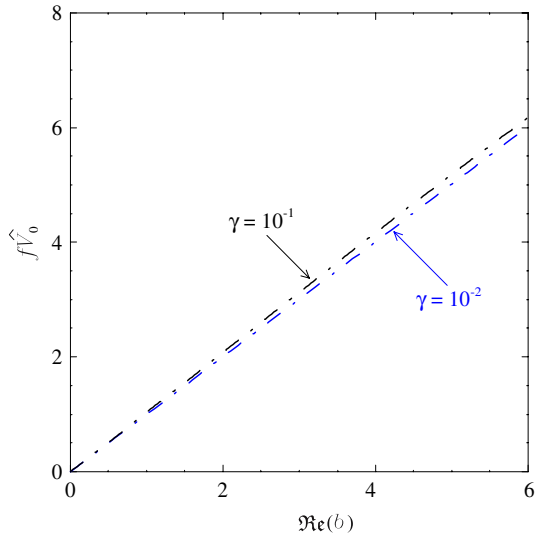

Fig. 3 Frictionless TEDI growth factors for force control (from [40])

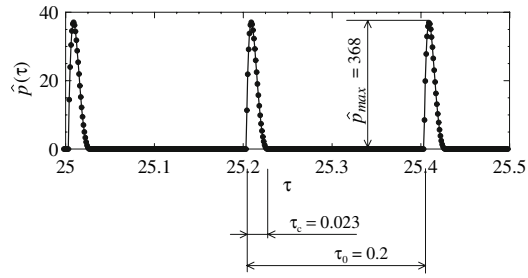

Fig. 4 The limit cycle for $\hat{p}$ for $\hat{V} = 1, \gamma = 10^{-1}$ when the layer is bonded to half-space A (from [39])

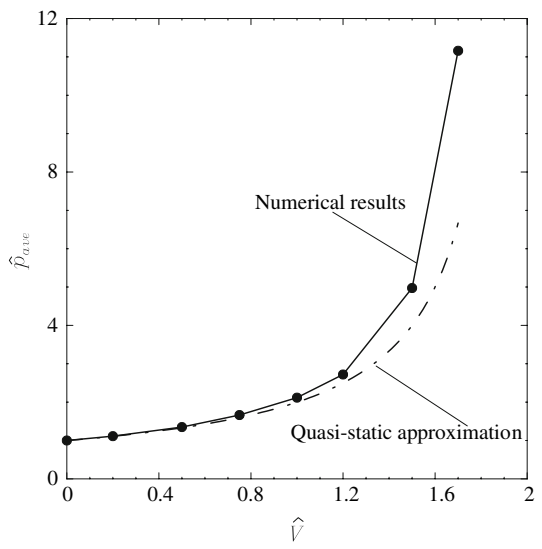

Fig. 5 Effect of dimensionless sliding speed $\hat{V}$ for $\gamma = 10^{-1}$ on the contact pressure $\hat{p}_{\text{ave}}$ averaged over the period $\hat{t}_0$ when the layer is bonded to half-space A (from [39])

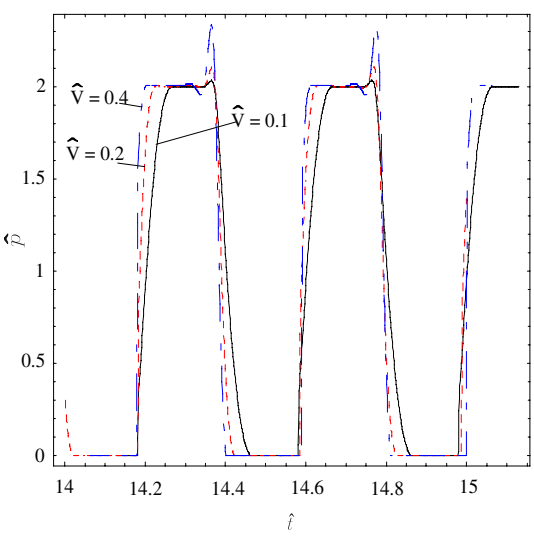

Fig. 6 Limit cycle for the contact pressure $\hat{p}$ when the layer is constrained to half-space A ($\gamma = 10^{-1}$ and $\hat{V} = 0.1, 0.2, 0.4$, from [40])

predicted by the quasi-static analysis is also shown for comparison). The two curves are quite close until we approach the quasi-static critical speed, implying that the limit cycle represents a nonlinear oscillation about the quasi-static solution.

In Fig. 6 the limit cycle for the contact pressure $\hat{p}$ is shown for the case in which we have a normal force ($\sigma(0, t) = -p_0$) prescribed at the end $x = 0$ of the layer. It would seem that the main effect, even in the limit of near-zero speed, is to produce a limit cycle with about $1/2$ of the period in separation, and $1/2$ under contact.

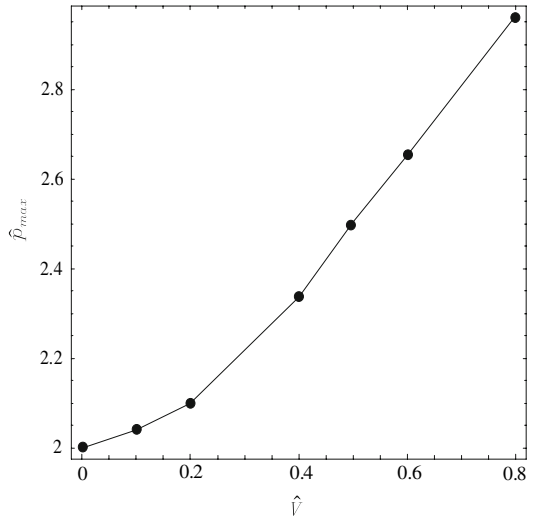

Fig. 7 Variation of $\hat{p}_{\max}$ with the speed $\hat{V}$ when the layer is constrained to half-space A ($\gamma = 10^{-1}$, from [40])

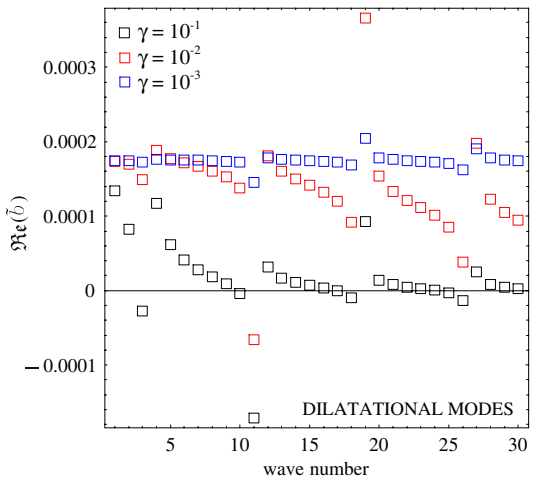

Fig. 8 Variation of the exponential growth rate $\Re\epsilon(\tilde{b})$ with the wave number for dilatational modes, different γ, $\nu = 0.3$, $H = 1$, $f = 0.1$, $\hat{V}_0 = 10^{-3}$, $\hat{p}_0 = 10^{-3}$ (NF–TD) (from [41])

As secondary effect, a localized maximum appears, and the period of the steady-state oscillation slightly increases with speed, with the contact phase one reducing and the maximum pressure growing sensibly.

In this case the average contact pressure in the period between successive impacts cannot change because it is imposed ($p_{\text{ave}} = p_0$). This is interesting, as the maximum contact pressure $\hat{p}_{\max}$ grows with the speed (Fig. 7). As expected, $\hat{p}_{\max}$ monotonically increases more than linearly with $\hat{V}$.

3.1.2 "Frictional" TEDI

Moving to the case in which frictional tractions are included, shear modes will interact with the jumping modes of the "frictionless TEDI".

In this section results of the linear perturbation analysis are presented for the NF–TD case. No significantly different result is obtained in the other cases of constraint.

In the purely dynamic case the only natural modes of vibration exist. When thermal effects are considered, the natural modes of vibration will be differently excited and for each possible frequencies we will have a different growth rate corresponding to an excited mode.

Figures 8 and 9 show the variation of the exponential growth rate $\Re\epsilon(\tilde{b})$ with the wave number for different γ and the first 30 dilatational and shear modes, respectively.

Reducing γ leads to dilatational growth rates moving upward and at small γ all modes show similar growth factors. Notice that relatively large values of growth rate are here associated with beating modes (for example dilatational mode $m = 3$ with shear mode $n = 6$, $m = 11$ with $n = 21$, and so on).

Figure 10 shows, in terms of $\hat{p}_0$ and $\hat{V}_0$, the zone in which shear effects dominate over dilatational ones ("shear" zone) and vice versa ("dilatational" zone). The solid line divides the "shear" zone from the "dilatational" one, whereas a dashed line allows to define where we can use the frictionless approximation. Shear effects can be significant at low pressures provided that the speed is sufficiently small. This figure is made by considering only the modes for which $\Re\epsilon(\tilde{b})$ is maximum (we considered the first 100 modes). The distinction between "shear" and "dilatational" zone will not be so clear. In fact, we expect the existence of a zone where shear and dilatational modes are competitive.

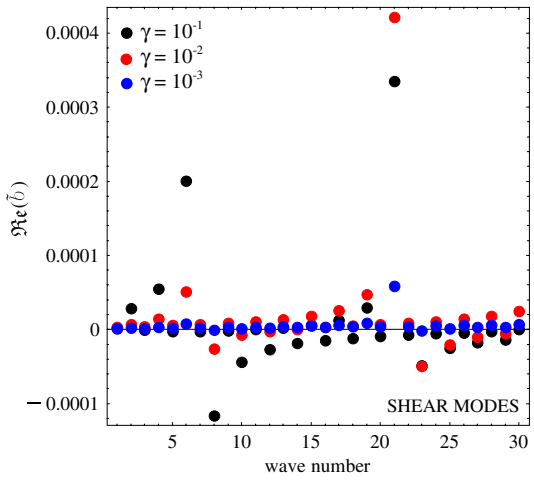

Fig. 9 Variation of the exponential growth rate $\Re\mathfrak{e}(\tilde{b})$ with the wave number for shear modes, different γ, $\nu = 0.3$, $H = 1$, $f = 0.1$, $\hat{V}_0 = 10^{-3}$, $\hat{p}_0 = 10^{-3}$ (NF–TD) (from [41])

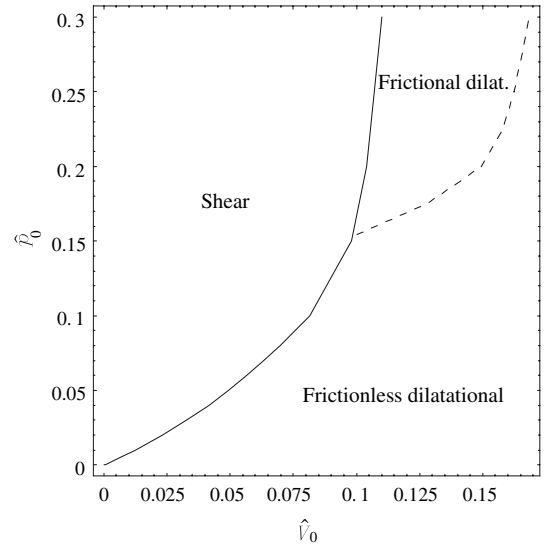

Fig. 10 Relation between $\hat{p}_0$ and $\hat{V}_0$ for which the shear maximum growth rate $\Re\mathfrak{e}(\tilde{b})_{\max}$ is larger than the dilatational one and vice versa (from [41])

Anyway, we can notice that shear-growth factors dominate the system behavior at low sliding speed, whereas dilatational ones dominate when higher speeds are considered. Also, shear-traction elastic waves significantly modify dilatational modes only at very high pressures. In fact, small differences with the growth rate of the first "frictionless TEDI" mode can be found in practical ranges of the contact pressure.

In the other cases (NF–TF, ND–TD and ND–TF) similar conclusions can be derived. However, when the normal displacement is constrained (ND–TD and ND–TF cases), additional eigenvalues with $\Im\mathfrak{m}(b) = 0$ (i.e., pure real) are found above a certain critical speed corresponding to the TEI modes. Naturally, above the TEI critical speed, the only possible steady state is with negative imposed displacement (otherwise there is seizure, i.e., an infinite increase of the pressure). TEI modes (real eigenvalues) dominate over TEDI ones at higher speed, whereas at low speed TEDI shear modes will characterize the system behavior.

The above results allow us to summarize the possible behaviors of the system:

- at very large pressure $\hat{p}_0$ shear modes dominate over dilatational ones, and the steady state will probably be governed by alternating periods of stick and slip;
- reducing the pressure to a condition in which shear and dilatational modes are competitive, separation phases will probably overlap with the periods of stick and slip;
- at low pressures dilatational modes are dominant. In such cases, the steady state will probably be characterized by alternating phases of contact and separation.

Figures 11 and 12, where the limit cycles of the speed $\hat{V}\left(\hat{t}\right)$ and contact pressure $\hat{p}\,(t)$ are, respectively, plotted for $\hat{V}_0 = 10^{-1}$ and $\hat{p}_0 = 10$ (here, the dimensionless factor 10 is somehow unrealistically large but shown only for representative purposes, since at smaller speeds similar results can be obtained), show the steady state is characterized by alternating periods of stick and slip. With a red line we plot the frictionless solution, i.e., the solution obtained by neglecting shear tractions elastic waves. The frictionless limit cycle for the pressure is very different, being constituted by alternating periods of contact and separation.

Figure 13 shows the fully established limit cycle of the dimensionless contact pressure $\hat{p}(\hat{t})$ for $\hat{V}_0 = 10^{-1}$ and $\hat{p}_0 = 1$. It is composed of four alternating periods of stick, slip, separation and slip again. During the stick phase we have a pick of pressure and the instantaneous speed $\hat{V}$ is zero. Obviously, the period between successive impacts

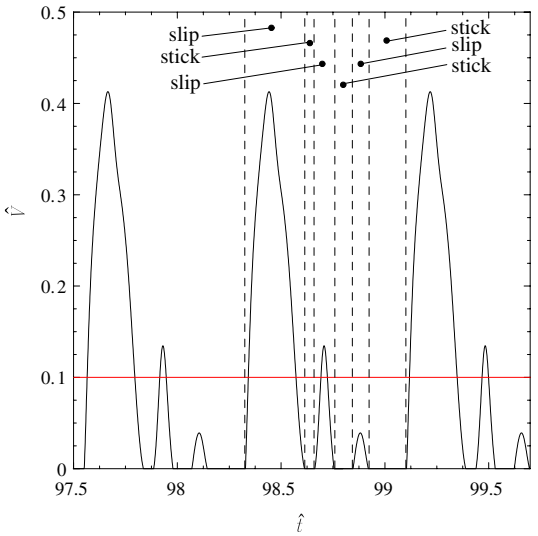

Fig. 11 The limit cycle of $\hat{V}$ for $\nu = 0.3$, $H = 1, \gamma = 10^{-1}$, $\hat{V}_0 = 10^{-1}$, $\hat{V}_0/\hat{p}_0 = 10^{-2}$ and $f = 0.1$

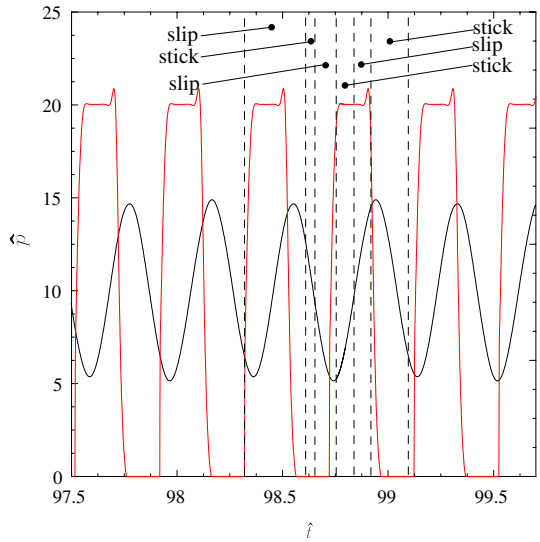

Fig. 12 The limit cycle of $\hat{p}$ for $\nu = 0.3$, $H = 1, \gamma = 10^{-1}$, $\hat{V}_0 = 10^{-1}$, $\hat{V}_0/\hat{p}_0 = 10^{-2}$ and $f = 0.1$

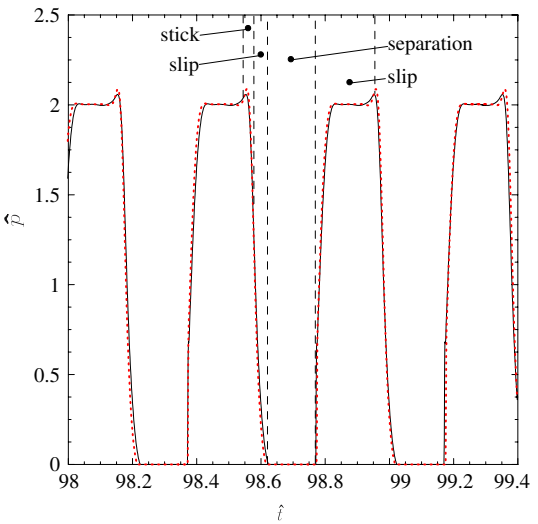

Fig. 13 The limit cycle of $\hat{p}$ for $\nu = 0.3$, $H = 1, \gamma = 10^{-1}$, $\hat{V}_0 = 10^{-1}$, $\hat{V}_0/\hat{p}_0 = 10^{-1}$ and $f = 0.1$ (from [41])

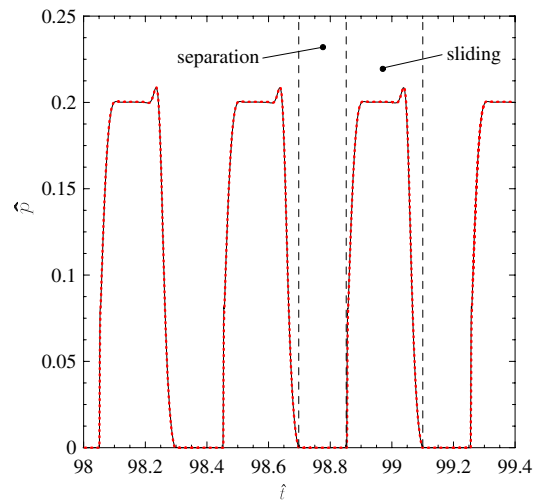

Fig. 14 The limit cycle for $\hat{p}$ for $\nu = 0.3$, $H = 1$, $\gamma = 10^{-1}$, $\hat{V}_0 = 10^{-1}$, $\hat{V}_0/\hat{p}_0 = 1$ and $f = 0.1$ (from [41])

is independent of $\hat{V}_0$ and given by $\hat{t}_0 = 4\gamma$. Now the frictionless limit cycle for the pressure (red dot line) is very close to the frictional one. Only a very small difference in the peak of the pressure can be noticed.

Reducing the pressure $\hat{p}_0$, i.e., thus increasing the ratio $\hat{V}_0/\hat{p}_0$, the dilatational modes will dominate the transient response of the system and the limit cycle will be similar to the frictionless case (red online version only dot line) with alternating periods of separation and sliding contact. This is confirmed in Fig. 14 where the limit cycle of $\hat{p}\,(t)$ is plotted for $\hat{V}_0 = \hat{p}_0 = 10^{-1}$.

4 Frictional TEDI: 2D problems

In this section we aim to discuss the coupled case for two-dimensional geometries. First we consider the case of two conducting and elastic sliding half-spaces studied in [45, Fig. 15]. Later we will discuss the case of a conducting elastic layer sliding between two layers which are also elastic and conducting studied in [46, Fig. 20].

4.1 Two elastic half-spaces

This is the equivalent of Adams' paper [47] of DI, with frictional heating added, or the equivalent of the paper by Burton et al. [28] regarding TEI, with inertia terms added. In the case without frictional heating [47], dynamic instability can only occur for different materials (for identical materials we have two Rayleigh waves of equal amplitude and equal wavelength but with 180 degree phase difference propagating in the same direction without interaction). When smooth-contact Stoneley waves exist for unbounded frictionless contacts without separation (i.e., when the shear-wave speeds of the contacting materials do not differ greatly) [48], instability occurs as f is increased from zero. For the other cases in which smooth-contact Stoneley waves do not exist (i.e., when the materials have significantly different shear-wave speeds), analogous waves appear at finite values of the friction coefficient. For the TEI, the critical speed is well defined and depends on the wavelength.

The governing equations for the problem under investigation (for plane-strain conditions) we write (see [45])

$$\frac{\partial^2\theta}{\partial x^2}+\frac{\partial^2\theta}{\partial y^2}-\frac{1}{k}\frac{\partial\theta}{\partial t}=0, \tag{15}$$

$$(\lambda+2\mu)\frac{\partial^2 u_x}{\partial x^2}+\mu\frac{\partial^2 u_x}{\partial y^2}+(\lambda+\mu)\frac{\partial^2 u_y}{\partial x\partial y}-m\frac{\partial\theta}{\partial x}-\rho\frac{\partial^2 u_x}{\partial t^2}=0, \tag{16}$$

$$(\lambda+\mu)\frac{\partial^2 u_x}{\partial x\partial y}+\mu\frac{\partial^2 u_y}{\partial x^2}+(\lambda+2\mu)\frac{\partial^2 u_y}{\partial y^2}-m\frac{\partial\theta}{\partial y}-\rho\frac{\partial^2 u_y}{\partial t^2}=0, \tag{17}$$

where $m=(3\lambda+2\mu)\alpha$.

One of two half-planes can be regarded as stationary and the other as moving at speed V_0. The perturbation moves at a speed v_1 over the stationary body and hence at a speed v_2 over the moving body in a material frame of reference such that $|v_1-v_2|=V_0$. There will be four mechanical boundary conditions on the friction surfaces. These entail continuity of the two tractions, continuity of normal displacement (full contact) and the Coulomb friction law:

$$u_{y_1}\big|_{y=0}-u_{y_2}\big|_{y=0}=0, \tag{18}$$

$$\sigma_{xy_1}\big|_{y=0}-\sigma_{xy_2}\big|_{y=0}=0, \tag{19}$$

$$\sigma_{yy_1}\big|_{y=0}-\sigma_{yy_2}\big|_{y=0}=0, \tag{20}$$

$$\sigma_{xy_1}\big|_{y=0}-f\,\sigma_{yy_1}\big|_{y=0}=0. \tag{21}$$

Also, there are two thermal boundary conditions which are continuity of temperature and the frictional-heating balance (for half-plane 1 the heat flow is positive if exiting the body, for half-plane 2 it is positive if entering the body):

$$\theta_1|_{y=0}-\theta_2|_{y=0}=0, \tag{22}$$

$$q_2-q_1-fVp=0, \tag{23}$$

where V is the instantaneous sliding speed defined as

$$V=V_0-\left(\frac{\partial u_{x_1}}{\partial t}-\frac{\partial u_{x_2}}{\partial t}\right). \tag{24}$$

In a way similar to that described in the previous section, the stability of the system can be studied by considering the possibility that a small perturbation in the temperature, stress and displacement fields can grow exponentially

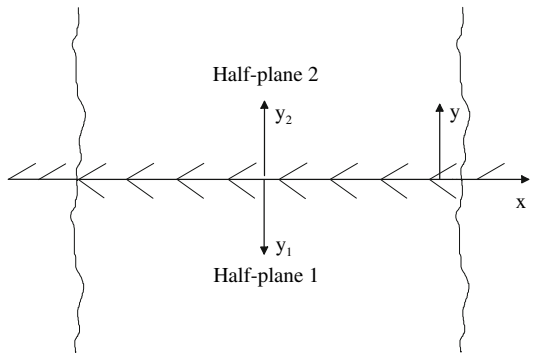

Fig. 15 Two elastic and conducting half-planes in sliding contact against each other (from [44])

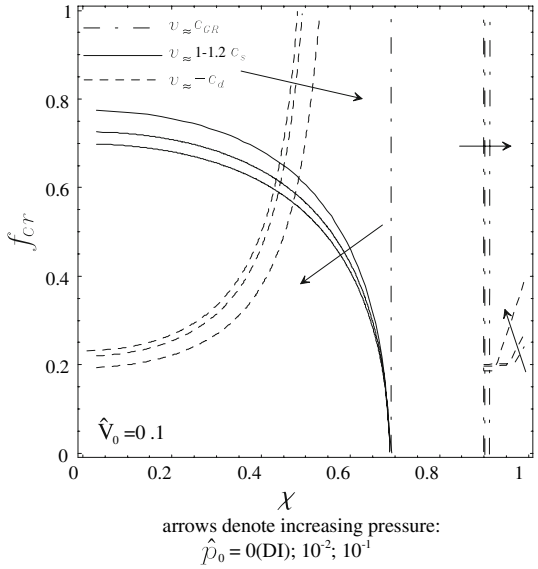

Fig. 16 Modification of DI stability boundaries with thermo-elastic effects (from [44])

in time. In the sequel we show that the instability boundary for DI and TEI modifies when thermo-elastic effects are added.

Figure 16 shows the modification of the DI critical friction coefficient when thermo-elastic effects are included (the parameter χ is defined as the ratio between the shear-wave speeds of the materials). The maps are obtained for $\hat{V}_0 = V_0/c_{s_1} = 10^{-1}$ (c_{s_1} is the shear-wave velocity in the material 1), and different $\hat{p}_0 = p_0/\mu_1$. A relatively weak coupling between thermal and dynamic effects exists. The boundary instability limits are plotted as solid and dashed lines for the waves traveling at the shear (c_{s_1}) and dilatational (c_{d_1}) waves speed, respectively. With a dashed–dot line we plot the stability boundary for the waves traveling at the Rayleigh wave speed (c_{GR_1}). Notice the unstable interfacial waves that travel at speed c_{d_1} move in the opposite direction.

In the range where smooth-contact Stoneley waves do not exist (large mismatch between the shear-wave speeds of the materials, i.e., small values of χ), the effect of thermal expansion can be explored through the variation of the critical coefficient for instability. Figure 17 shows the modification of the DI critical-friction coefficient with thermo-elastic effects in this case. Where the smooth-contact Stoneley waves exist and the critical friction coefficient is zero, the only comparison which can be done must be the effect on the growth rate for a given f or V_0. Therefore, Fig. 18 shows that the dimensionless growth rate $\tilde{b} = bk_1/c_{s_1}^2$ changes with the friction coefficient f. In this case smooth-contact Stoneley waves exist and they are the only unstable waves for small friction coefficient. In fact, a TEI disturbance has positive growth rates only when $f \gtrsim 0.19$ and the waves which propagate at a speed very close to, but slightly lower than c_{d_1} in the negative x-direction are unstable for $f \gtrsim 0.3$. Notice that the exponential growth rate of these unstable waves reduces with the pressure $\hat{p}_0$.

Figure 19 shows the effect of the inertia terms in the TEI maps. Significant deviations are noticed when $\hat{V}_0$ approaches unity and larger wave numbers are considered. Notice, however, that, surprisingly, inertia terms tend to decrease the instability range.

4.2 An elastic and conducting layer sliding between two elastic and conducting layers

Figure 20 shows the geometry of the problem under investigation.

By applying symmetric or antisymmetric boundary conditions, the problem can be reduced to a two-layer model in which a half-layer is sliding against another layer. Yi [46] developed a finite-element procedure to solve the

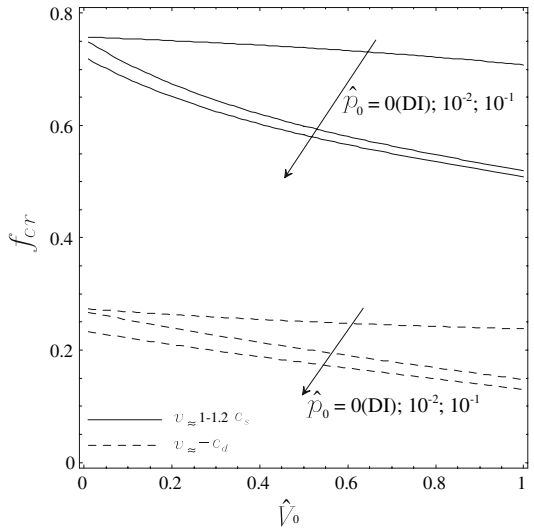

Fig. 17 Modification of DI critical friction coefficient with thermo-elastic effects (from [44])

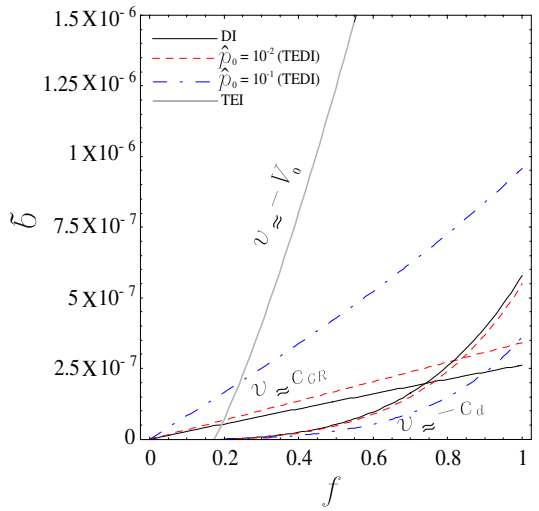

Fig. 18 Variation of the exponential growth rate $\tilde{b}$ with the friction coefficient for small mismatch between the shear-wave speeds ($\chi = 0.9$) and different $\hat{p}_0$ (from [44])

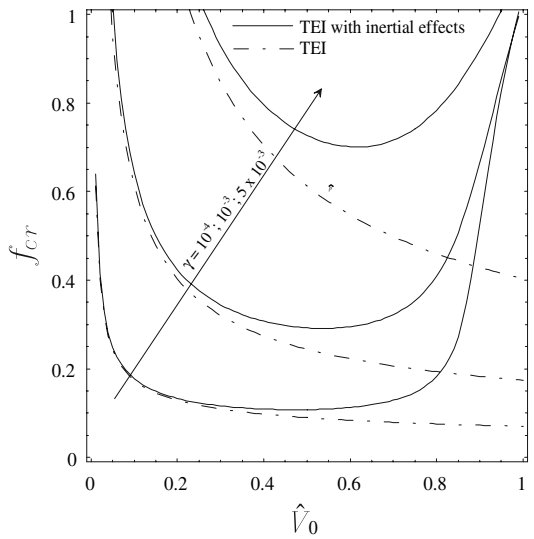

Fig. 19 Modification of TEI stability boundaries with elastodynamic effects ($\chi = 0.2$) (from [44])

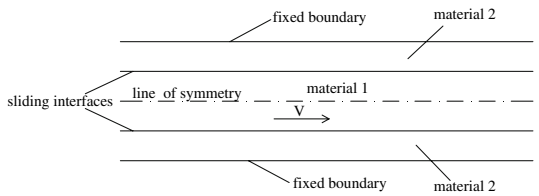

Fig. 20 An elastic and conducting layer sliding between two elastic and conducting layers

problem involving thermo-elastodynamic instability. Notice the system investigated by Yi [46] falls in the category of "frictionless" TEDI models.

Figures 21 and 22 (corresponding to Figs. 4 and 5 of Yi's paper) show the growth rate as a function of sliding speed for the wave number for which the system has the lowest critical TEI speed and under antisymmetric and symmetric boundary conditions. Notice, as the real part of b is always positive, that this is also true at arbitrarily small speed. In the phase in which we have only TEDI instability, $\mathfrak{Re}\,(b)$ is very small (of the order of 10^{-5}) and remains approximately constant with the speed; in the second phase, the growth rate increases with the sliding

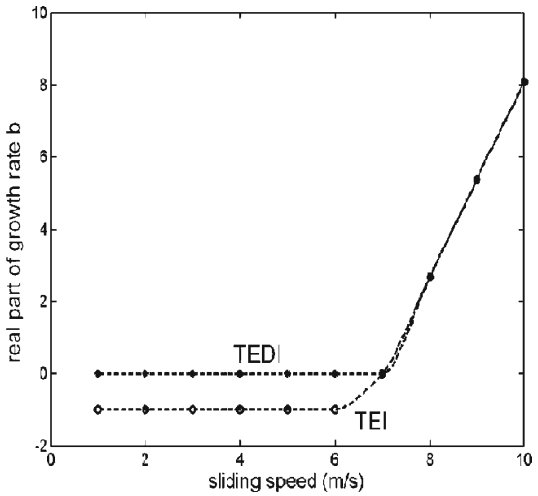

Fig. 21 Variation of the growth rate with the sliding speed for antisymmetric b.c. (from [46])

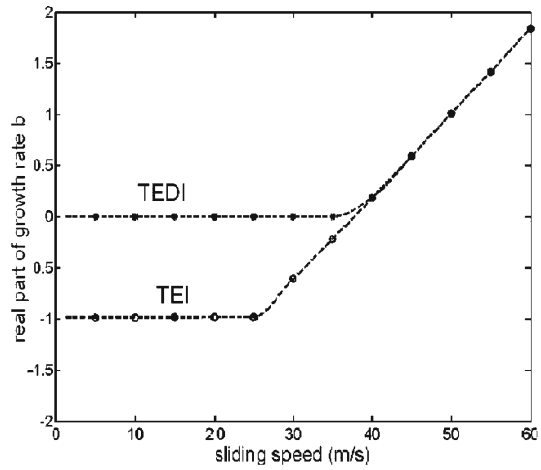

Fig. 22 Variation of the growth rate with the sliding speed for symmetric b.c. (from [46])

speed and we do not discern TEDI and TEI results. The transition point of the two phases in TEDI corresponds to the critical sliding speed in TEI.

Investigation of the imaginary part of the growth rate reveals that the leading modes of TEDI vibrate at very high frequencies (comparable with the frequencies of DI). This means that the leading modes are induced by dynamic effects, with small but non-negligible growth rates. When the sliding speed exceeds the critical TEI speed, the imaginary parts of the leading modes are comparable with those of TEI modes.

Hence, at low sliding speeds we have some coupling between dynamic and thermo-elastic effects, but at high sliding speeds this coupling is negligible and thermo-elastic effects dominate.

5 Conclusions

Frictional instabilities in the sliding of elastic bodies are of interest in a wide range of scientific and industrial applications. For example, many of the aspects of earthquake phenomena can apparently be explained by frictional stability regimes; frictional instabilities are generally held responsible for squeal; the formation of hot spots is a consequence of frictionally excited thermo-elastic instability (TEI); frictional-instability phenomena cause Schallamach waves; stick–slip instabilities are also studied in the Atomic Friction Microscope.

In particular, both frictional dynamic (DI) and thermo-elastic (TEI) instabilities can be analyzed using linear perturbation methods, leading to a characteristic equation for the exponential growth rate of an initial perturbation. Thermo-elastic deformations are neglected in the analysis of frictional instabilities and a quasi-static approximation is used in the analysis of TEI. Some justification for this 'decoupling' of the two phenomena is provided by the widely divergent time scales involved. Thermo-elastic instabilities occur on the rather slow time scale of thermal diffusion, whereas elastodynamic processes are governed by the elastic wave speeds in the materials.

Therefore, we were motivated to develop an analysis of the coupled problem including both elastodynamic and thermo-elastic effects in the same perturbation analysis. The resulting studies, however, found results which are more interesting than what we expected to find in our original motivation, namely, we found a new family of instabilities, named TEDI.

This investigation was initiated by considering a one-dimensional elastic layer bonded to a rigid half-space and sliding against a second rigid half-space and a 2D problem of half-planes and layers in sliding contact.

For the simple 1D model, with constant coefficient of friction, the model without coupling shows a trivial response: no dynamic instability, whereas a frictional-heating (TEI) instability is obtained only for high speeds and due to displacement constraint of the model (in the case of force control, no TEI instability would be present). The coupled model leads to instability at all speeds, and at small speeds the nonlinear limit cycle obtained is clearly an oscillation closer to the quasi-static approximation, but with a "jumping" mode of impacts possibly responsible for noise and vibrations. These instabilities were called "frictionless TEDI" since they emerge already when we neglect the effect of shear deformations (i.e., shear-wave propagation).

An improvement of the model by including shear-traction elastic waves at the interface permits to include the possibility of stick–slip deformations. In this case, shear waves interact with dilatational waves and hence the resulting behavior is more complicated: the "frictionless TEDI" modes are reduced or completely suppressed. For this reason, we called these new modes "frictional TEDI" modes.

In particular, starting from very high ratios between the sliding speed V_0 and applied pressure p_0, dilatational modes dominate over shear modes and the steady state is characterized by alternating phases of sliding contact and separation (similarly to the "frictionless TEDI" case). Reducing the sliding speed (or increasing the pressure p_0) to a condition in which shear and dilatational modes are competitive, separation phases overlap with the periods of stick and slip. At low ratios V_0/p_0 shear modes dominate over dilatational ones, and the steady state is governed by alternating periods of stick and slip.

Notice in the limit of small pressures or high speeds, the "frictionless TEDI" case is recovered. Hence, "frictionless TEDI" correctly describes the system behavior when the ratio V_0/p_0 is sufficiently high.

For 2D models the full study shows a relatively weak effect of the thermal deformations. In fact, for two in-plane sliding half-spaces only with high sliding speeds (comparable to the wave speeds in the material) does some significant variation of the growth factor emerge. However, in a layered 2D geometry the coupling is again significant at low sliding speeds (the real part of the growth rate b is always positive also at arbitrarily small speed).

Limiting the attention to the present models of TEDI, there are a number of interesting effects which it may be important to include in the future. The most important is probably *damping*, both internal and structural. Damping would possibly be significant to reduce TEDI, or completely suppress it. Some preliminary judgment on which class of instability would be affected by damping would be important, particularly as there are many forms of damping. Probably some experimental evidence would be needed, to avoid generating an endless number of complicated purely mathematical formulations. Another form of damping might be that due to more complex forms of friction laws, but it will be sensible to limit such a study to the forms of TEDI where it is known that a friction law related to the classical Coulomb law can lead to significantly different results. For example, only the ill-posed TEDI solution can be significantly affected by a rate-state-dependent friction law, since these are generally used exactly within the scope of regularizing ill-posed DI solutions.

References

1. Ben-Zion Y (2001) Dynamic ruptures in recent models of earthquake faults. J Mech Phys Solids 49:2209–2244
2. Rice JR, Lapusta N, Ranjith K (2001) Rate and state dependent friction and the stability of sliding between elastically deformable solids. J Mech Phys Solids 49:1865–1898
3. Barquins M, Koudine AA, Vallet D (1996) On the existence of Schallamach waves during surface friction in rubber-like material as a function of thickness. Comptes Rendu Mecanique 323:433–438
4. Fosberry RAC, Holubecki Z (1961) Disc brake squeal: its mechanism and suppression. Technical Report. Motor Industry Research Association. Warwickshire, England
5. Spurr RT (1961) A theory of brake squeal. Proc Inst Mech Engrs (Auto Div) 1:33–52
6. Hoffmann N, Gaul L (2004) A sufficient criterion for the onset of sprag-slip oscillations. Arch Appl Mech 73(9–10):650–660
7. Leine RI, Brogliato B, Nijmeijer H (2002) Periodic motion and bifurcations induced by the Painlevé paradox. Eur J Mech A/Solids 21(5):869–896
8. Leine RI, Brogliato B, Nijmeijer H (2004) Periodic motion and bifurcations induced by the Painlevé paradox, in advanced dynamics and control of structures and machines, Irschik H, Schlacher K (eds) CISM Courses and Lectures Vol 444, pp 169–194
9. Sampson JB, Morgan F, Reed DW, Muskat M (1943) Friction behavior during the slip portion of the stick-slip process. J Appl Phys 14(12):689–700

10. Rabinowicz E (1958) The intrinsic variables affecting the stick-slip process. Proc Phys Soc London 471: 668–675
11. Bell R, Burdekin M (1969-1970) A study of the stick-slip motion of machine tool feed drives. Proc Inst Mech Eng 184(1):543–557
12. Hess DP, Soom A (1990) Friction at lubricated line contact operating at oscillating sliding velocities. ASME J Tribol 112:147–152
13. Hunt JB, Torbe I, Spencer GC (1965) The phase-plane analysis of sliding motion. Wear 8(6):455–465
14. Popp K (1992) Some model problems showing stick-slip motion and chaos. In: Friction-induced vibration, chatter, squeal, and chaos, vol 49. American Society of Mechanical Engineers, pp 1–12
15. Tolstoi DM (1967) Significance of the normal degree of freedom and natural normal vibrations in contact friction. Wear 10:199–213
16. Godfrey D (1967) Vibration reduced metal-to-metal contact and causes an apparent reduction in friction. ASLE Trans 10:183–192
17. Sakamoto T (1987) Normal displacement and dynamic friction characteristics in a stickslip process. Tribol Int 20(1):25–31
18. Barber JR (1969) Thermoelastic instabilities in the sliding of conforming solids. Proc Roy Soc A312:381–394
19. Kennedy FE, Ling FF (1974) A thermal, thermoelastic and wear simulation of a high energy sliding contact problem. ASME J Lub Tech 96:497–507
20. Floquet A, Dubourg MC (1994) Non-axisymmetric effects for 3D thermal analysis of a brake. ASME J Tribol 116:401–408
21. Bryant MD, Wang JP, Lin JW (1995) Thermal mounding in high speed dry sliders – Experiment, theory and comparison. Wear 181:668–677
22. Kao TK, Richmond JW, Douarre A (2000) Brake disc hot spotting and thermal judder: an experimental and finite element study. Int J Vehicle Des 23:276–296
23. Kreitlow W, Schrödter F, Matthäi H (1985) Vibration and hum of disc brakes under load. SAE 850079
24. Inoue H (1986) Analysis of brake judder caused by thermal deformation of brake disk rotors. SAE 865131
25. Zagrodzki P (1990) Analysis of thermomechanical phenomena in multidisc clutches and brakes. Wear 140: 291–308
26. Anderson AE, Knapp RA (1989) Hot spotting in automotive friction systems. In: International Conference on wear of materials, Vol. 2, 673–680
27. Lee K, Dinwiddie RB (1998) Conditions of frictional contact in disk brakes and their effects on brake judder. SAE 980598
28. Burton RA, Nerlikar V, Kilaparti SR (1973) Thermoelastic instability in a seal-like configuration. Wear 24:177–188
29. Dow TA, Stockwell RD (1977) Experimental verification of thermoelastic instabilities in sliding contact. ASME J Lub Tech 99:359–364
30. Banerjee BN, Burton RA (1979) Experimental studies on thermoelastic effect in hydrodynamically lubricated face seals. ASME J Lub Tech 101:275–282
31. Lee K, Barber JR (1993) Frictionally-excited thermoelastic instability in automotive disk brakes. ASME J Tribol 115:607–614
32. Johansson L (1993) Model and numerical algorithm for sliding contact between two elastic half-planes with frictional heat generation and wear. Wear 160:77–93
33. Zagrodzki P, Lam KB, Al-Bahkali E, Barber JR (1999) Simulation of a sliding system with frictionally-excited thermoelastic instability. Thermal Stresses, Cracow, Poland
34. Yi Y-B, Barber JR, Zagrodzki P (2000) Eigenvalue solution of thermoelastic instability problems using Fourier reduction. Proc Roy Soc (London) A 456: 2799–2821
35. Yi Y-B, Barber JR (2001) HotSpotter: a finite element software package for evaluating the susceptibility of axisymmetric multidisk brakes and clutches to thermoelastic instability (TEI). http://www-personal.engin.umich.edu/∼jbarber/hotspotter.html
36. Biot MA (1956) Thermoelasticity and irreversible thermodynamics. J Appl Phys 27:240–253
37. Lessen M (1956) Thermoelasticity and thermal shock. J Mech Phys Solids 5:57–61
38. Carlson DE (1972) Linear thermoelasticity. In: Flugge S (ed) Handbuch der Physik, vol VIa/2. Springer-Verlag, Berlin pp 297–345
39. Afferrante L, Ciavarella M, Barber JR (2006) Sliding thermoelastodynamic instability. S Proc Roy Soc A 462:2161–2176
40. Afferrante L, Ciavarella M (2006a) A note on ThermoElastoDynamic Instability (TEDI) for a 1D elastic layer: force control. Int J Solids Struct 44(5):1380–1390
41. Afferrante L, Ciavarella M (2006b) "Frictionless" and "frictional" ThermoElastic Dynamic Instability (TEDI) of sliding contacts. J Mech Phys Solids 54(11):2330–2353
42. Afferrante L, Ciavarella M (2005) Instabilità Termo-Elasto-Dinamica (TEDI): come il calore per attrito instabilizza i modi di vibrare elastodinamici in un semplice modello monodimensionale. In: AIAS XXXIV Convegno Nazionale - 14–17 settembre 2005, Milano
43. Barber JR, Dundurs J, Comninou M (1980) Stability considerations in thermoelastic contact. ASME J Appl Mech 47:871–874
44. Afferrante L, Ciavarella M (2006) ThermoElastic and Dynamic Instability (TEDI) in sliding systems. In: Mota Soares CA et al (eds), III European conference on computational mechanics solids, structures and coupled problems in engineering, Lisbon, Portugal, 5–8 June 2006
45. Afferrante L, Ciavarella M (2007) Thermo-Elastic Dynamic Instability (TEDI) in frictional sliding of two elastic halfspaces. J Mech Phys Solids 55(4):744–764
46. Yi Y-B (2006) Finite element analysis of the thermoelastodynamic instability involving frictional heating. ASME J Tribol 128:718–724
47. Adams GG (1995) Self-excited oscillations of two elastic half-spaces sliding with a constant coefficient of friction. ASME J Appl Mech 62:867–872
48. Achenbach JD, Epstein HI (1967) Dynamic interaction of a layer and a half-space. ASCE J Eng Mech Div EM5:27–42